The 8th European Congress on Computational Methods in Applied Sciences and Engineering
ECCOMAS Congress 2022
5-–9 June 2022, Oslo, Norway

NUMERICAL SIMULATION OF MULTIPHASE FLOWS WITH INCOMPRESSIBLE VISCOELASTIC FLOWS AND ELASTIC SOLIDS

ALEXANDRE CABOUSSAT[1], LEO DISERENS[1,2] AND MARCO PICASSO[2]

[1] Geneva School of Business Administration (HEG), University of Applied Sciences and Arts Western Switzerland (HES-SO), alexandre.caboussat@hesge.ch, leo.diserens@hesge.ch

[2] Institute of Mathematics, Ecole polytechnique fédérale de Lausanne, 1015 Lausanne, Switzerland, marco.picasso@epfl.ch, leo.diserens@epfl.ch

Key words: Free surface flows, viscoelastic fluids, elastics solids, multiphase flows, rheologies

Abstract. A numerical model for the simulation of multiphase flows with free surfaces is presented. The model allows to incorporate in a unified manner several phases ranging from incompressible Newtonian flows, Oldroyd-B viscoelastic flows and neo-Hookean elastic solids deformations.

We advocate a Eulerian modeling of the multiphase flows, relying on the volume fraction of liquid, describing multiple phases with those different rheologies. One advantage of the Eulerian approach is to allow for large deformations of elastic solids, and changes of topologies. The numerical framework relies on an operator splitting strategy and a two-grid method. The numerical model is validated with a numerical experiment based on the collision between two elastic bodies with free surfaces.

1 MATHEMATICAL MODELING

Multiphase flows are ubiquitous in nature. The objective of this work is to introduce a unified mathematical model for the numerical simulation of multiphase flows with free surfaces, including multiple immiscible phases with different rheologies. The rheologies we would like to consider are those of Newtonian fluids, of visco-elastic fluids, but also of elastic solids. Our goal is to be able to account for large deformations or changes of topology of each phase. For this reason, we advocate an Eulerian framework based on a volume-of-fluid approach [5, 6, 7]. This framework has been experimented for various multiphysics problems [1, 2, 3], and is extended here to elastic materials as well.

Let $\Lambda \in \mathbb{R}^3$ be a cavity containing a multiphase liquid flow and ambient air, and let $T > 0$ be the final time of the simulation. The free surface model we consider reads as follows. The volume fraction of liquid [5, 7] is used to track each of the liquid phases. We consider the characteristic function of each liquid $\varphi_\ell : \Lambda \times (0,T) \to \{0,1\}$, $\ell = 1, \dots, N$, where N is the total number of phases, and

$$\varphi(\mathbf{x},t) = \sum_{\ell=1}^{N} \varphi_\ell(\mathbf{x},t).$$

Since the phases are immiscible, we have $\varphi(\mathbf{x},t) \in \{0,1\}$, for all $\mathbf{x} \in \Lambda$ and for all $t \in (0,T)$. Let us then define:

$$\begin{aligned} \Omega_\ell(t) &= \{\mathbf{x} \in \Lambda \ : \ \varphi_\ell(\mathbf{x},t) = 1\}, \\ \Omega(t) &= \bigcup_{\ell=1}^{N} \Omega_\ell(t) = \{\mathbf{x} \in \Lambda \ : \ \varphi(\mathbf{x},t) = 1\}, \end{aligned}$$

and Q_T, the space-time domain containing the liquids is defined by $Q_T = \big\{(\mathbf{x},t) \in \Lambda \times (0,T) : \varphi(\mathbf{x},t) = 1\big\} = \big\{\mathbf{x} \in \Omega(t),\ t \in (0,T)\big\}$.

Let us consider a velocity field $\mathbf{v} : Q_T \to \mathbb{R}^3$, a pressure field $p : Q_T \to \mathbb{R}$ and an extra-stress tensor $\boldsymbol{\sigma} : Q_T \to \mathbb{R}^{3\times 3}$ in the liquid phases. In order to describe the kinematics of the free surface, each characteristic function φ_ℓ (the volume fraction of liquid for the phase ℓ) satisfies (in a weak sense) a transport equation:

$$\frac{\partial \varphi_\ell}{\partial t} + \mathbf{v} \cdot \nabla \varphi_\ell = 0 \qquad \text{in } \Lambda \times (0,T), \quad \ell = 1, \ldots, N. \tag{1}$$

This equation translates the fact that the fluid particles move at velocity $\mathbf{v}$. The characteristic functions φ_ℓ are given at initial time, and boundary conditions are imposed on the inlet boundary (if any).

Within this multiphase flow, we would like to consider a mixture of liquid phases with different rheologies. A unified model is derived, which allows to consider the interaction between Newtonian fluids, visco-elastic fluids and elastic solids, with free surfaces. We assume that the velocity $\mathbf{v}$, the pressure p, and the extra-stress tensor $\boldsymbol{\sigma}$ satisfy the following set of equations in the multiphase flow domain $\Omega(t)$ for all $t \in (0,T)$:

$$\rho(\varphi)\left(\frac{\partial \mathbf{u}}{\partial t} + (\mathbf{u}\cdot\nabla)\mathbf{u}\right) - \nabla \cdot (2\eta_s(\varphi)\boldsymbol{\epsilon}(\mathbf{u}) - p\mathbf{I}_d + \boldsymbol{\sigma}) = \rho(\varphi)\mathbf{g}, \quad \text{in } \Omega(t), \tag{2}$$

$$\nabla \cdot \mathbf{u} = 0, \quad \text{in } \Omega(t), \tag{3}$$

$$\alpha(\varphi)\boldsymbol{\sigma} + \lambda(\varphi)\left(\frac{\partial \boldsymbol{\sigma}}{\partial t} + (\mathbf{u}\cdot\nabla)\boldsymbol{\sigma} - \nabla\mathbf{u}\boldsymbol{\sigma} - \boldsymbol{\sigma}\nabla\mathbf{u}^T\right) = 2\eta_p(\varphi)\boldsymbol{\epsilon}(\mathbf{u}), \quad \text{in } \Omega(t). \tag{4}$$

Here $\mathbf{D}(\mathbf{v}) = 1/2(\nabla\mathbf{v} + \nabla\mathbf{v}^T)$ is the symmetric deformation tensor, $\mathbf{I}_d$ the identity tensor, and $\mathbf{g}$ denotes the gravity field. The physical quantities are the density ρ, the solvent viscosity $\eta_s \geq 0$, the polymer viscosity $\eta_p > 0$ and the relaxation time $\lambda \geq 0$. They are assumed to vary from one liquid phase to another as discontinuous, piecewise constant, functions of the volume fractions of liquid φ_ℓ, $\ell = 1, \ldots, N$. For the sake of simplicity, the notation $\rho(\varphi)$ actually denotes $\rho(\varphi_1, \ldots, \varphi_N)$. The parameter α is a modeling parameter that also depends on the phase.

A 2D sketch of the situation is illustrated in Figure 1 in the case of two colliding droplets in vacuum.

Equations (2)(3) are the Navier-Stokes equations for incompressible flows with the addition of an extra-stress tensor. Equation (4), with $\alpha = 1$ is the so-called Oldroyd-B model for visco-elastic flows [1]. Actually, this model allows to unify Newtonian fluids (when $\alpha = 1$ and $\lambda = 0$)

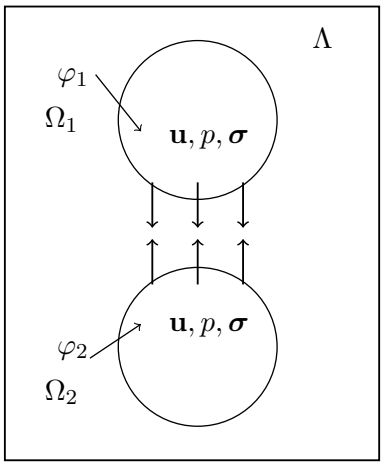

Figure 1: Colliding droplets with different rheologies. 2D sketch of the geometrical domain. Two droplets composed of two different immiscible liquid phases (tracked by φ_1 and φ_2) are colliding in a cavity Λ. The droplets are surrounded by vacuum. The velocity, pressure and extra-stress variables $(\mathbf{u}, p, \boldsymbol{\sigma})$ are defined in both liquid phases.

[7], visco-elastic fluids (when $\alpha = 1$ and $\lambda > 0$) [1], and elastic solids expressed in Eulerian coordinates (when $\alpha = 0, \lambda > 0$, and $\eta_s = 0$) [9]. In the latter case, the tensor $\boldsymbol{\sigma}$ represents the stress of an incompressible Neo-Hookean elastic solid. The ratio η_p/λ is then equal to the Lamé coefficient of the incompressible solid material [9].

This system of equations (1)–(4) is supplemented by initial conditions at time $t = 0$ for the volume fractions of liquid, the velocity and the extra-stress tensor. The initial fluid regions are defined as $\Omega_\ell(0) = \{\mathbf{x} \in \Lambda; \varphi_\ell(\mathbf{x}, 0) = 1\}$ and $\Omega(0) = \{\mathbf{x} \in \Lambda; \varphi(\mathbf{x}, 0) = 1\}$. Boundary conditions on $\partial\Lambda$ for the velocity include slip or no-slip conditions. If an inflow is imposed, additional inflow boundary conditions for the the volume fractions of liquid, the velocity and the extra-stress tensor must be prescribed on the inflow boundary of $\partial\Lambda$.

Surface tension effects on the liquid-vacuum interface are not taken into account, and the surrounding vacuum has no influence on the fluid. The boundary conditions on the liquid-vacuum interface $\partial\Omega(t)\backslash\partial\Lambda$ are then given by the no-force boundary condition:

$$(-p\mathbf{I} + 2\eta_s\boldsymbol{\epsilon}(\mathbf{u})) + \boldsymbol{\sigma}) \cdot \mathbf{n} = \mathbf{0}, \tag{5}$$

where $\mathbf{n}$ is the external normal vector to the liquid-vacuum interface.

2 NUMERICAL ALGORITHM

The numerical algorithm follows [6] and relies on a time splitting algorithm and a two-grid method. The order one splitting algorithm relies on a decoupling between advection and diffusion phenomena.

2.1 Time splitting strategy

Let $0 = t^0 < t^1 < t^2 < \ldots < t^N = T$ be a subdivision of the time interval $[0, T]$ and $\Delta t^n = t^n - t^{n-1}$, $n = 0, 1, 2, \ldots, N-1$ be the time steps. Let φ_ℓ^{n-1}, $\mathbf{u}^{n-1}, p^{n-1}, \boldsymbol{\sigma}^{n-1}$ be approximations of φ_ℓ, $\mathbf{u}$, p, $\boldsymbol{\sigma}$ respectively available at time t^{n-1}, and $\varphi^{n-1} = \sum_{\ell=1}^N \varphi_\ell^{n-1}$.

Let $\Omega^{n-1} = \{\mathbf{x} \in \Lambda : \varphi^{n-1}(\mathbf{x}) = 1\}$ be the approximated liquid region at time t^{n-1}. The approximations φ_ℓ^n, φ^n, $\mathbf{u}^n$, p^n, $\boldsymbol{\sigma}^n$ at time t^n are computed by means of the splitting algorithm illustrated in Figure 2.

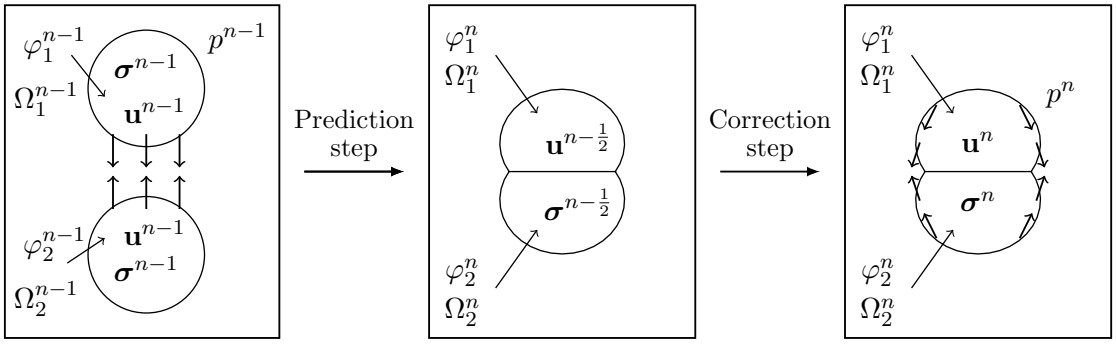

Figure 2: Time splitting algorithm from time t^{n-1} to t^n (left to right). At each time step $n-1$, we first solve the advection equations (6) (7) (8) to obtain the new positions of the liquid phases Ω_1^n and Ω_2^n and predictions $\mathbf{u}^{n-1/2}$ and $\boldsymbol{\sigma}^{n-1/2}$. Then, the diffusion problems (a generalized Stokes problem and the Oldroyd-B problem) are solved to obtain the corrected velocity $\mathbf{u}^n$, the pressure p^n, and the corrected extra-stress tensor $\boldsymbol{\sigma}^n$

1. The prediction step consists in solving between t^{n-1} and t^n the advection problems

$$\frac{\partial \varphi_\ell}{\partial t} + \mathbf{u} \cdot \nabla \varphi_\ell = 0, \quad \ell = 1, \ldots, N, \tag{6}$$

$$\frac{\partial \mathbf{u}}{\partial t} + (\mathbf{u} \cdot \nabla)\mathbf{u} = 0, \tag{7}$$

$$\frac{\partial \boldsymbol{\sigma}}{\partial t} + (\mathbf{u} \cdot \nabla)\boldsymbol{\sigma} = 0. \tag{8}$$

   to obtain the approximations $\varphi_\ell^n, \varphi^n = \sum_{\ell=1}^N \varphi_\ell^n$, $\Omega_\ell^n = \{\mathbf{x} \in \Lambda : \varphi^n(\mathbf{x}) = 1\}$, $\Omega^n = \bigcup_{\ell=1}^N \Omega_\ell^n$, and the predictions $\mathbf{u}^{n-\frac{1}{2}}$ and $\boldsymbol{\sigma}^{n-\frac{1}{2}}$ in Ω^n.

2. The correction step consists in solving between t^{n-1} and t^n in Ω^n the diffusion problems:

$$\rho(\varphi^n)\frac{\partial \mathbf{u}}{\partial t} - \nabla \cdot (2\eta_s(\varphi^n)\boldsymbol{\epsilon}(\mathbf{u}) - p\mathbf{I}_d + \boldsymbol{\sigma}) = \rho(\varphi^n)\mathbf{g}, \tag{9}$$

$$\nabla \cdot \mathbf{u} = 0, \tag{10}$$

$$\alpha(\varphi^n)\boldsymbol{\sigma} + \lambda(\varphi^n)\left(\frac{\partial \boldsymbol{\sigma}}{\partial t} - \nabla \mathbf{u}\boldsymbol{\sigma} - \boldsymbol{\sigma}\nabla \mathbf{u}^T\right) = 2\eta_p(\varphi^n)\boldsymbol{\epsilon}(\mathbf{u}). \tag{11}$$

2.2 Two-grid method

The splitting algorithm allows to decouple the diffusion and advection phenomena. In order to take further advantage of this situation, two grids are used for the space discretization, following [7]. They are illustrated in Figure 3 (in two space dimensions): a regular grid of small structured cells (left) is used to solve the advection problems (6)–(8), while an unstructured tetrahedral finite element mesh (right) is used to solve the diffusion problem (9)-(11).

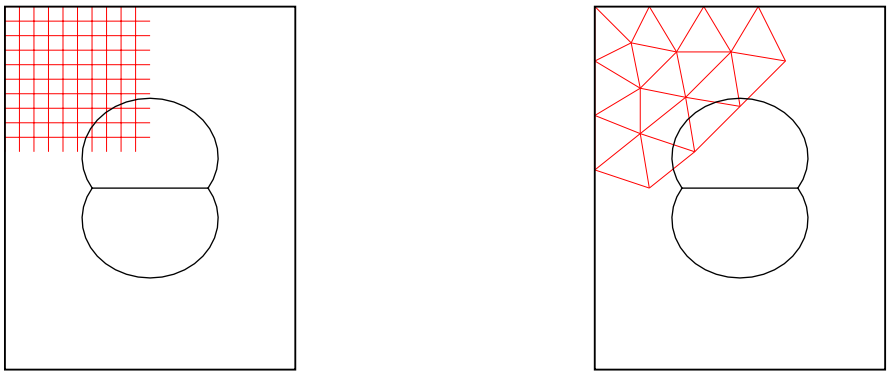

Figure 3: Two-grid method (2D sketch). The advection problems are solved on a structured grid of small cells (left). The diffusion problems are solved on a coarser unstructured finite element mesh (right).

The structured grid is chosen to be finer than the finite element grid, in order to improve the accuracy of the free surfaces and interfaces' approximation. The advection problems (6)–(8) are solved with a forward characteristics method [7, 10]. Interface reconstruction techniques, such as a SLIC method [8], or mass conservation heuristics [6], are added to avoid numerical diffusion when implementing (6), as φ_ℓ is discontinuous across the interfaces. On the other hand, the unstructured finite element mesh allows to consider complex geometries, and is considered coarser to keep the computational cost of solving the diffusion (Stokes) problem reasonable. A semi-implicit Euler scheme in time, and stabilized, continuous, piecewise linear, finite elements are used to solve (9)-(11) [4].

We typically advocate $H \simeq 3h - 5h$ in the numerical experiments presented below for a balance between accuracy and computational efficiency. Under the CFL condition, the overall convergence rate of the numerical method is one. Thus, when dividing H, h and Δt by two, the error should be divided by two.

3 PRELIMINARY NUMERICAL RESULTS

Some preliminary results are presented here, involving multiphase flows with a free surface. We consider the case of two elastic (rubber) balls of different densities and rigidity with radius $r = 0.1$ [m], and centers $(-0.15, 0, 0)$ and $(0.15, 0, 0)$ respectively. They are colliding in a cavity $\Lambda = (-0.43, 0.27) \times (-0.14, 0.14) \times (-0.14, 0.14)$ filled with vacuum. The physical parameters are $\eta_{s,1} = \eta_{s,2} = 0$ [Pa s], $\rho_1 = 1000$ [kg m^{-3}], $\rho_2 = 2000$ [kg m^{-3}], $\lambda_1 = \lambda_2 = 10^{-2}$ [s],

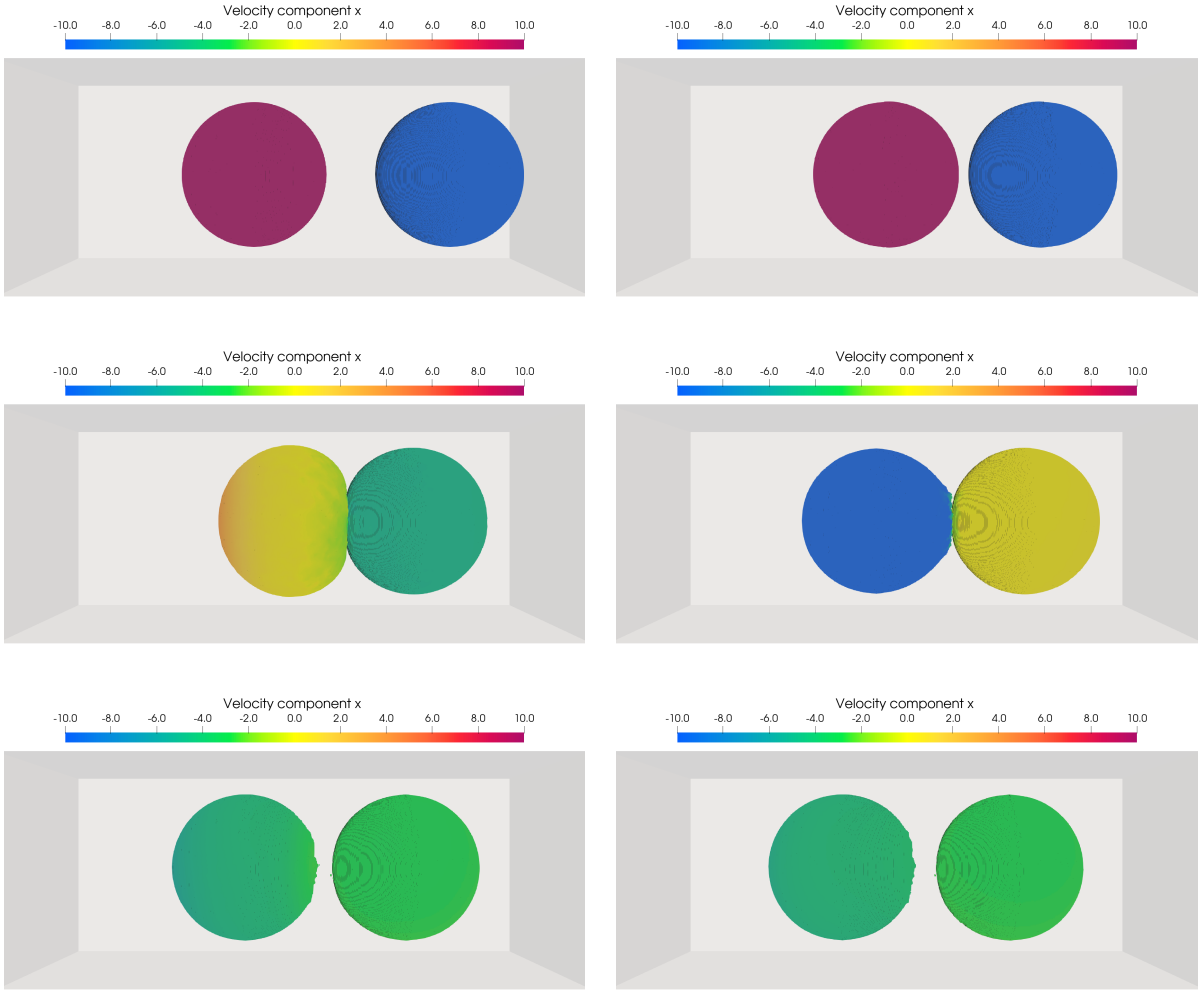

Figure 4: Colliding elastic balls, with a light ball (left) and a heavier ball (right). Snapshots of the collision at times $t = 0, 3, 6, 10, 15$ and 20 [ms] (left to right, top to bottom).

$\eta_{p,1} = 4 \cdot 10^4$ [Pa s], and $\eta_{p,2} = 2 \cdot 10^5$ [Pa s]. There are no gravity forces. The modeling parameters are $\alpha_1 = \alpha_2 = 0$, which implies that both balls are composed of elastic materials. The phases are initiated with an horizontal velocity along Ox of 10 [m/s] in opposite direction. The initial extra-stress tensor $\boldsymbol{\sigma}(0)$ is equal to zero. Figure 4 shows snapshots of the collision at times $t = 0, 3, 6, 10, 15$ and 20 [ms]. It shows that the light ball is propelled back to the left after impact, while the dense one continues its march to the left as well. Figure 5 shows horizontal profiles along the line Ox (for $y = z = 0$), at time $t = 6$ [ms] of the horizontal component of the velocity $\mathbf{u}_x$ and of the $\boldsymbol{\sigma}_{xx}$ extra-stress tensor component for three time and space discretizations (coarse, middle and fine, $h = 4, 2, 1$ [mm], $H = 16, 8, 4$ [mm], $\Delta t = 0.4, 0.2, 0.1$ [ms] respectively). One can observe visually a convergence towards a given profile.

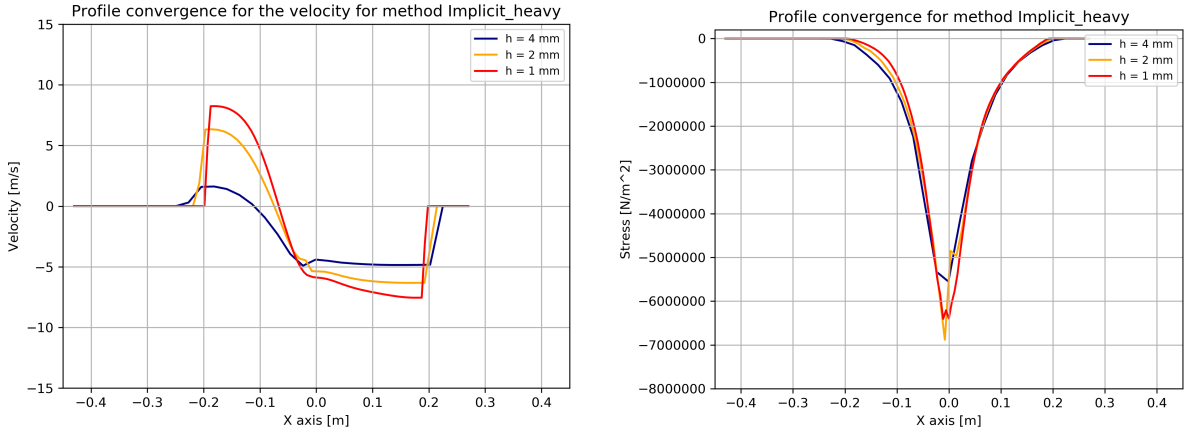

Figure 5: Horizontal profiles along the horizontal line x at time $t = 6$ [ms] of the horizontal component of the velocity $\mathbf{u}_x$ (left) and of the $\boldsymbol{\sigma}_{xx}$ extra-stress tensor component (right). Three time and space discretizations are considered (coarse, middle and fine, $h = 4, 2, 1$ [mm], $H = 16, 8, 4$ [mm], $\Delta t = 0.4, 0.2, 0.1$ [ms]).

4 CONCLUSIONS

We have introduced a unified mathematical model for incompressible Newtonian fluids, incompressible viscoelastic fluids and elastic solids with free surfaces. Our formulation allows to include multiple immiscible phases and free surfaces with the ambient air considered as vacuum. We have extended an existing numerical method to include such cases with various rheologies. The algorithm relies on a time splitting algorithm for the time discretization, and a two-grid approach for the space discretization. Preliminary results have been presented when two elastic bodies are colliding in a vacuum, and some convergence results have been exhibited. Future work will investigate the interactions when the multiple phases have very different rheologies.

REFERENCES

[1] A. Bonito, M. Picasso, and M. Laso. Numerical simulation of 3D viscoelastic flows with free surfaces. *J. Comput. Phys.*, 215(2):691–716, 2006.

[2] Sebastien Boyaval, Alexandre Caboussat, Arwa Mrad, Marco Picasso, and Gilles Steiner. A semi-lagrangian splitting method for the numerical simulation of sediment transport with free surface flows. *Computers and Fluids*, 172:384–396, 2018.

[3] A. Caboussat, J. Hess, A. Masserey, and M. Picasso. A numerical model for the simulation of shallow laser surface melting. In *Proceedings of the II International Conference on Simulation for Additive Manufacturing Sim-AM 2019*, pages 286–296, 2019.

[4] L. P. Franca and S. L. Frey. Stabilized finite element method: II. the incompressible Navier-Stokes equations. *Comp. Meth. Appl. Mech. Engrg*, 99:209–233, 1992.

[5] C. W. Hirt and B. D. Nichols. Volume of fluid (VOF) method for the dynamics of free boundaries. *J. Comput. Phys.*, 39(1):201–225, 1981.

[6] N. James, A. Caboussat, S. Boyaval, and M. Picasso. Numerical simulation of 3D free surface flows, with multiple incompressible immiscible phases. Applications to impulse waves. *International Journal for Numerical Methods in Fluids*, pages 00:1–24, 2014.

[7] V. Maronnier, M. Picasso, and J. Rappaz. Numerical simulation of three dimensional free surface flows. *Int. J. Num. Meth. Fluids*, 42(7):697–716, 2003.

[8] W. F. Noh and P. Woodward. SLIC (simple line interface calculation). *Proceedings of the Fifth International Conference on Numerical Methods in Fluid Dynamics*, 59:330–340, 1976.

[9] M. Picasso. From the free surface flow of a viscoelastic fluid towards the elastic deformation of a solid. *Comptes Rendus. Math.*, 354:543–548, 2016.

[10] O. Pironneau. On the transport-diffusion algorithm and its applications to the Navier-Stokes equations. *Numer. Math.*, 38(3):309–332, 1981/82.